Indian Journal of Chemical Technology
Vol. 28, May 2021, pp. 274-284

Coupling system of silver carbonate nanoparticles and bismuth oxyiodide nanosheets with enhanced photocatalytic properties

Xianyi Lv, Dongfang Zhang* & Jiaxun Wang

Department of Chemistry, College of Science, Huazhong Agricultural University, Wuhan 430 070, PR China

E-mail: zdfbb@mail.hzau.edu.cn

Received 15 September 2020; accepted 7 April 2021

In this work, silver carbonate nanoparticles and BiOI nanosheets have been prepared separately and binary Ag_2CO_3/BiOI composite are synthesized via a facile solvo thermal method. The as-prepared materials have been well characterized using techniques covering X-ray diffraction (XRD), energy dispersive X-ray spectroscopy (EDX), transmission electron microscopy (TEM), High-resolution transmission electron microscopy (HRTEM), ultraviolet-visible (UV-vis) diffuse reflectance spectroscopy, X-ray photoelectron spectroscopy (XPS), Photoluminescence (PL) emission spectroscopy. The photocatalytic activity of the as-synthesized materials has been evaluated for degrading various model pollutants (methyl orange, phenol and p-nitroaniline). It has been found that the incorporation of co-catalyst BiOI could promote the catalytic activity of Ag_2CO_3 and suppress the serious photocorrosion of Ag_2CO_3. Thus the Ag_2CO_3/BiOI composite showed excellent catalytic recycling stability. Moreover, the underlying mechanism has been investigated through radical trapping experiments. The results demonstrate that photoinduced holes are the main active species. The improvement in activity of Ag_2CO_3/BiOI could be attributed to the charge transfer between the heterojunction. Also, its good stability and reusability establish its promising potential for catalytic applications.

Keywords: Bismuth oxyiodide, Charge carrier, Heterojunction, Photocatalytic, Silver carbonate

Over the last years, population explosion and industrialization are the major factors responsible for the shortage of energy supply as well as the adverse impacts on environment. Environmental problems such as water contamination are becoming more and more troublesome, which result in major threats to ecological system[1-9]. Moreover, these harmful substances due to the discharge of wastewater are difficult to biodegrade and accumulate over a long period of time, which inevitably poses a threat to human beings once these toxic contaminants released into water body. The emergence of semi conductor photocatalysis has continued to receive wider acceptance as a promising way for environmental purification[10-14]. In the framework of limited water resources, it is indispensable and urgent to seek for green and recyclable solutions to deal with the toxic organics arising from wastewater.

The development of visible light sensitive photocatalysts has been a hot topic for researchers in recent times, such as BiOX(X=Cl, Br, I), g-C_3N_4, AgCl and Ag_2CO_3 (Ref. 5-20). They can absorb and highly utilize solar energy and are widely used to decompose organic pollutants. As a semiconductor material, Ag_2CO_3 owes the characteristic of excellent visible light responsive ability. However, there are still exist short comings for Ag_2CO_3crystal such as low separation efficiency of photoinduced holes and electrons as well as long-term catalytic activity is not ideal, which limiting its practical application in the advanced treatment of organic pollutants or minimize the risk of toxic chemicals.

Asa series of the visible-light driven photocatalysts, Bi-based materials have attracted much attention due to their low-cost, nontoxicity, chemical stability. Among them, the reported monoclinic bismuth oxyiodide (BiOI) with relative narrow band gap (E_g~1.90 eV) can be used for the dye decolorization because of its strong oxidizability and fast mobility[21]. The performance of photocatalyst is closely related to the separation efficiency and oxidation ability of photogenerated carriers. Methods to study the lifetime prolonging of photogenerated carriers and promoting the carrier transport process of BiOI include impurity doping, noble metal sensitization, and formation of heterojunction structures. In general, semiconductor combination with matching energy band gaps can induce a heterojunction between two different semiconductors. It is an efficient

way to inhibit the recombination rate of photo-induced carries and to enhance the photocatalytic efficiency of a single component.

In this study, heterostructures of coupled Ag_2CO_3/BiOI with pure Ag_2CO_3 and BiOI were synthesized via solvo thermal approach. The prepared materials were thoroughly characterized using various analytical techniques. Their application as photocatalyst, were examined in photodegradation of selected toxic organics such as methyl orange (MO), phenol and p-nitroanaline (PNA) under visible light. A remarkable photodegradation efficiency of Ag_2CO_3/BiOI composite was observed, which completely degraded 15 ppm of MO after 80 min with high stability over nine successive cycles. Furthermore, the Ag_2CO_3/BiOI composite exhibited remarkably improved photocatalytic activity along with favorable photostability compared to Ag_2CO_3 alone. The significantly enhanced photoactivity of Ag_2CO_3/BiOI composite was attributed to both of the heterostructure that promoted the separation of photoinduced carriers and sufficient visible-light harvesting capability.

Experimental Section

Material and photocatalyst synthesis

All reagents were analytical grade and used without further purifying. Ethylene glycol, PVP, $AgNO_3$, $NaHCO_3$, KI and $Bi(NO_3)_3{\cdot}5H_2O$ were used as feedstocks. In a typical procedure, weight of 1.94 g Bi $(NO_3)_3{\bullet}5H_2O$ plus 20 mL of deionized water and magnetically stir for 30 min, then add 2ml of ethylene glycol, 0.1 gPVP, 0.66 gKI and magnetically stir for 30 min. Transfer to a 50 ml reaction kettle, add ultra pure water to nearly full, and react in an oven at 120°C for 8 h. After the reaction is completed, the mixture is transferred to a beaker for centrifugal drying and grinding to obtain a BiOI product. For the synthesis of Ag_2CO_3 sample, 10 mL of 0.1 mol/L $NaHCO_3$ solution and 40 mL of 0.05 mol/L $AgNO_3$ solution were prepared. Take 9 mL $NaHCO_3$ solution and add 1.5 mL ethylene glycol for ultrasonic dispersion for 30 min. Then 36 mL of $AgNO_3$ solution was added for magnetic stirring reaction for 5 h, then drying in oven at 150°C for 3 h, centrifugal washing, drying and grinding to obtain the Ag_2CO_3 product. The Ag_2CO_3/BiOI catalyst was prepared via an in situ self-assembled hydrothermal synthesis procedure. Namely, 1.056 g BiOI plus 30 mL of deionized water was ultrasonically dispersing for 30 min, then adding 0.25 g $NaHCO_3$ plus 2 mL of ethylene glycol, magnetically stirring for 30 min, 1.02 g of $AgNO_3$ plus 50 mL of deionized water were slowly added into the above reaction solution and stirred for another 20 min to form a yellow mixture. Afterwards, the resulted solution was sealed in a 100 mL Teflon-lined stainless auto-calve and heated at the temperature of 170°C for 6.0 h. The prepared solution was allowed to cool down the room temperature naturally. The gray precipitate was repeatedly centrifuged, washed with alcohol and water for several times. Furthermore, the powders were obtained by grinding the collected composite dried in an air oven at 150°C for 3 h.

Characterizations

The crystal structures of BiOI, Ag_2CO_3 and fabricated Ag_2CO_3/BiOI samples were determined using X-ray powder diffraction (XRD) patterns by a diffractometer (Rigaku D/Max 2500v/pc) with Cu-Kα radiation (λ= 0.15406 nm). The morphologies and crystal structures of the photocatalysts were verified by transmission electron microscope(TEM, Titan the mis 200/Talos 200/ tecnai G2 F30 (FEI)).The optical response ranges of the samples were observed through diffuse reflectance spectra detected by a Varian CARY 500 UV-vis-NIR spectrophotometer equipped with a $BaSO_4$ integrating sphere as reference. X-ray photoelectron spectroscope (XPS, Escalab 250Xi (Thermo Scientific)) with the Al Kα radiation was performed to investigate the binding energies of Bi, I, O, C and Ag. The recombination rates of all samples were measured by the Photoluminescence (PL) spectra via a fluorescence spectrophotometer (Shimadzu RF-5301 PC, JP) at the excitation wavelength of 412 nm.

Photocatalysis experiments

The photocatalytic activities of the as-prepared BiOI, Ag_2CO_3 and Ag_2CO_3/BiOI samples were investigated by the degradation of MO, phenol and PNA solutions (15 ppm) at the room temperature. A 300 W Xenon lamp with a band-pass filter (λ≥420 nm) was used as the light source. Firstly, 30 mg of the catalyst sample was added into a reaction bottle filled with 150 ml of aqueous MO solution, and the mixture was magnetically stirred for in the darkness to enable adsorption-desorption equilibrium. Place the reaction bottle in a photoreaction instrument and irradiate for 60-80 min under Xenon lamp. Every 10 min, a certain amount of supernatant (ca. 3 mL) was taken and the catalyst powders were completely removed by centrifugation for 2 min at a speed of 10000 r/min. And the

photocatalytic degradation of phenol, PNA solution were also done follow the above steps. The concentration of MO, phenol or PNA in solution was analyzed through an UV-vis spectrophotometer (Nicolet 300 evolution).Cycling photocatalytic experiments were also carried out to test the recyclability of catalyst. During each cycle, the photocatalytic material was centrifuged and dried at 100 °C for 3 h. Then the recovered photocatalyst was used for the next cycle and the lost portion of catalyst was balanced by the addition of fresh. The experiments were repeated several times until nine cycles of degradation reactions.

Results and Discussion

Structure, property and morphology

The structural configuration of BiOI, Ag_2CO_3 or Ag_2CO_3/BiOI were explored by EDX spectra and corresponding elemental mapping images of C, Ag, O, Bi, and I in Ag_2CO_3/BiOI composite are shown in Fig. 1A-D. As can be seen, the BiOBr sample has component of Br, O and Bi element peaks, whereas only C, Ag and O peaks are present in Ag_2CO_3. The as-made Ag_2CO_3/BiOI composite contains mainly Bi, C, I, Ag and O elements. The phase and crystallization properties of photocatalyst were determined by XRD analysis. Fig. 1E is the x-ray

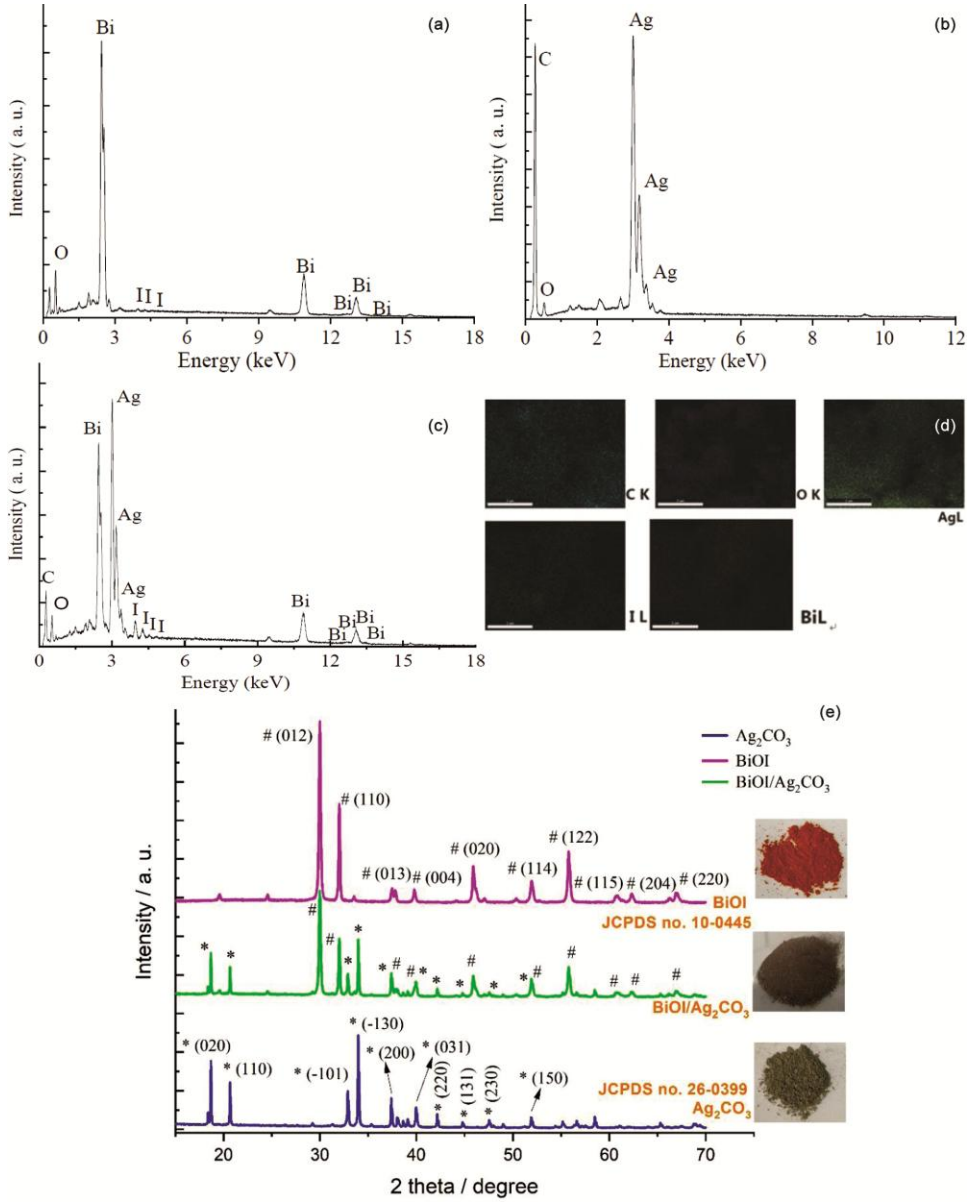

Fig. 1 — EDX spectra and of (a) pure BiOI; (b) Ag_2CO_3 and (c) Ag_2CO_3/BiOI samples as well as (d) elemental mapping images and (e) XRD patterns.

diffraction patterns of the prepared silver carbonate, bismuth oxyiodide and bismuth oxyiodide/silver carbonate compsoite. As can be seen, the first pink spectral line is the XRD pattern of BiOI, and it is obvious that there are several dominant peaks appear at 29.9°C, 32.0°C, 45.8°C, 55.7°C corresponding to (012), (110), (020) and (122) crystal planes of bismuth oxyiodide nanoparticles and this crystalline peak were well matched with the JCPDs card number 10-0445 of the tetragonal phase BiOI[22]. In addition, the sharp peaks of Ag_2CO_3 sample is well indexed to monoclinic structure of Ag_2CO_3 (PDF#26-0339), and the diffraction pattern of BiOI/Ag_2CO_3 composite also shows the crystalline Ag_2CO_3 and BiOI characteristic peaks, and conforms to the each position of standard diffraction peak. These strong diffraction peaks in the figure are sharp, indicating that the synthesized sample has good crystallinity. It can be determined from the XRD patterns that the as-prepared Ag_2CO_3, BiOI and Ag_2CO_3/BiOI were indeed the required samples. Moreover, morphology and microstructure of synthesized samples were further investigated by TEM and high-resolution TEM (HRTEM) images, as displayed in Fig. 2. From Fig. 2(a), it can be observed that a large number of irregular spheroid-like Ag_2CO_3 particles having a size of about 30-60 nm. In Fig. 2(b), a large number of irregular layered objects and the nanosheet/platelet shape structure of BiOI can be observed. In Fig. 2(c), it can be clearly seen that Ag_2CO_3 particles are tightly attached to the layered BiOI, anchored at the edge or surface of BiOI nanosheets, which indicates that heterojunction has been generated, which is helpful for the transfer of photo-generated electrons and for improving photocatalytic performance. Besides, Ag_2CO_3 nanoparticles that assembled in situ onto the surface of the BiOI sheet were not agglomerated as obvious as pure Ag_2CO_3, and the size of these Ag_2CO_3 nanoparticles that adhered to the BiOI nanosheets can remarkably decreased to about 15-40 nm. And under high resolution TEM (Fig. 2(d)), it was obvious to observe the lattice fringe spacing of 0.280 and 0.199 nm, which attributed to BiOI (110) and (020) planes, respectively. The legible lattice fringes in the HRTEM images implied the good crystallinity property of the tetragonal phase BiOI component. In detail,the d spacing values of 0.265 and 0.227 nm corresponded to the (-130) and (031)lattice planes of

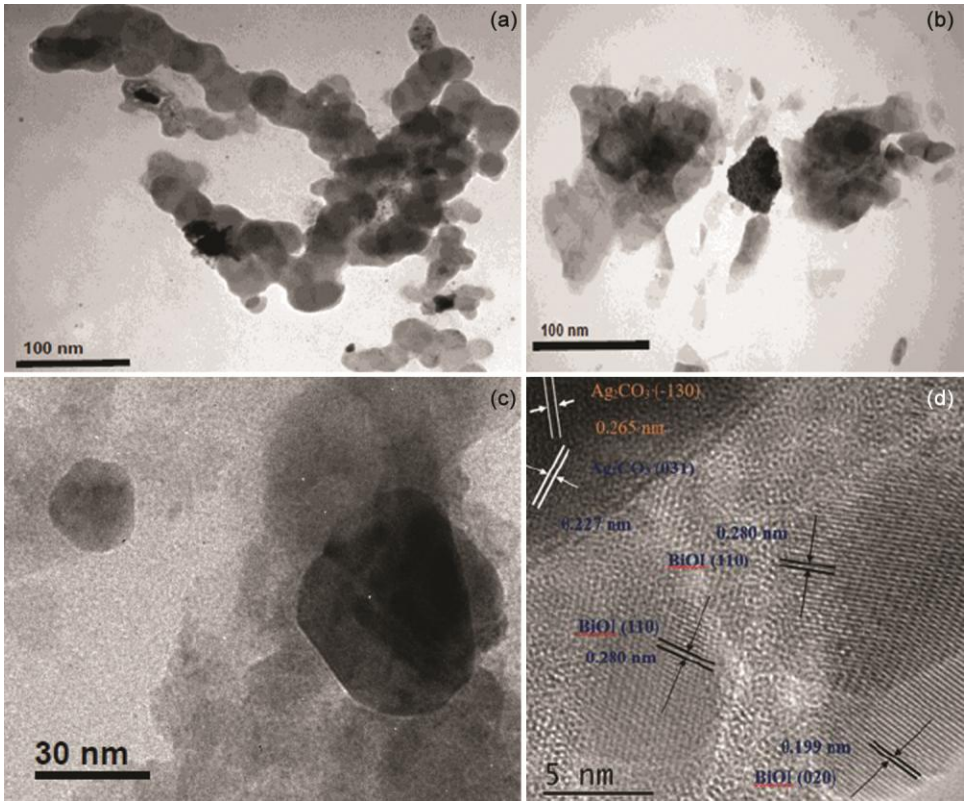

Fig. 2 — Representative TEM images of as-prepared (a) pure Ag_2CO_3, (b) BiOI, (c) Ag_2CO_3/BiOI and HRTEM image of (d) Ag_2CO_3/BiOI samples.

monoclinic Ag_2CO_3, respectively. Above results revealed that Ag_2CO_3 nanoparticles have been loaded on BiOI surface closely, which suggests that a heterojunction can be formed between the interfaces of BiOI and Ag_2CO_3. This firmly contact will create an opportunity for charge separation, which could promote the transfer of photoinduced electrons and reduce the recombined probability of electrons and holes.

The chemical constituents of different elements in Ag_2CO_3/BiOI composite photocatalysts verified by XPS were shown in Fig. 3. Survey spectrum (Figure 3a) indicated the existence of O, Ag, Bi, C and iodine elements in the composite. In the high-resolution XPS spectrum of I 3d (Fig. 3b), there are two evident peaks at 630.9 and 619.5 eV, which could be assigned to the spin orbital separation energy levels of I $3d_{3/2}$ and I $3d_{5/2}$ of negative monovalent iodine ion, respectively. Similarly, the two peaks at 158.9.1 and 164.2 eV corresponded to Bi $4f_{7/2}$ and Bi $4f_{5/2}$ of positive trivalent bismuth ion in Fig. 3(c), respectively. In Fig. 3(d), the binding energy peak of 'silver' in Ag_2CO_3/BiOI composite appears at 373.9 eV and 367.9 eV corresponding to Ag $3d_{3/2}$ and Ag $3d_{5/2}$ peaks with the separation of 6.0 eV for Ag (+1) configuration. The high-resolution XPS spectrum of O 1s (Fig. 3e) could be fitted by three individual peaks. The peak at 533.3 and 532.3

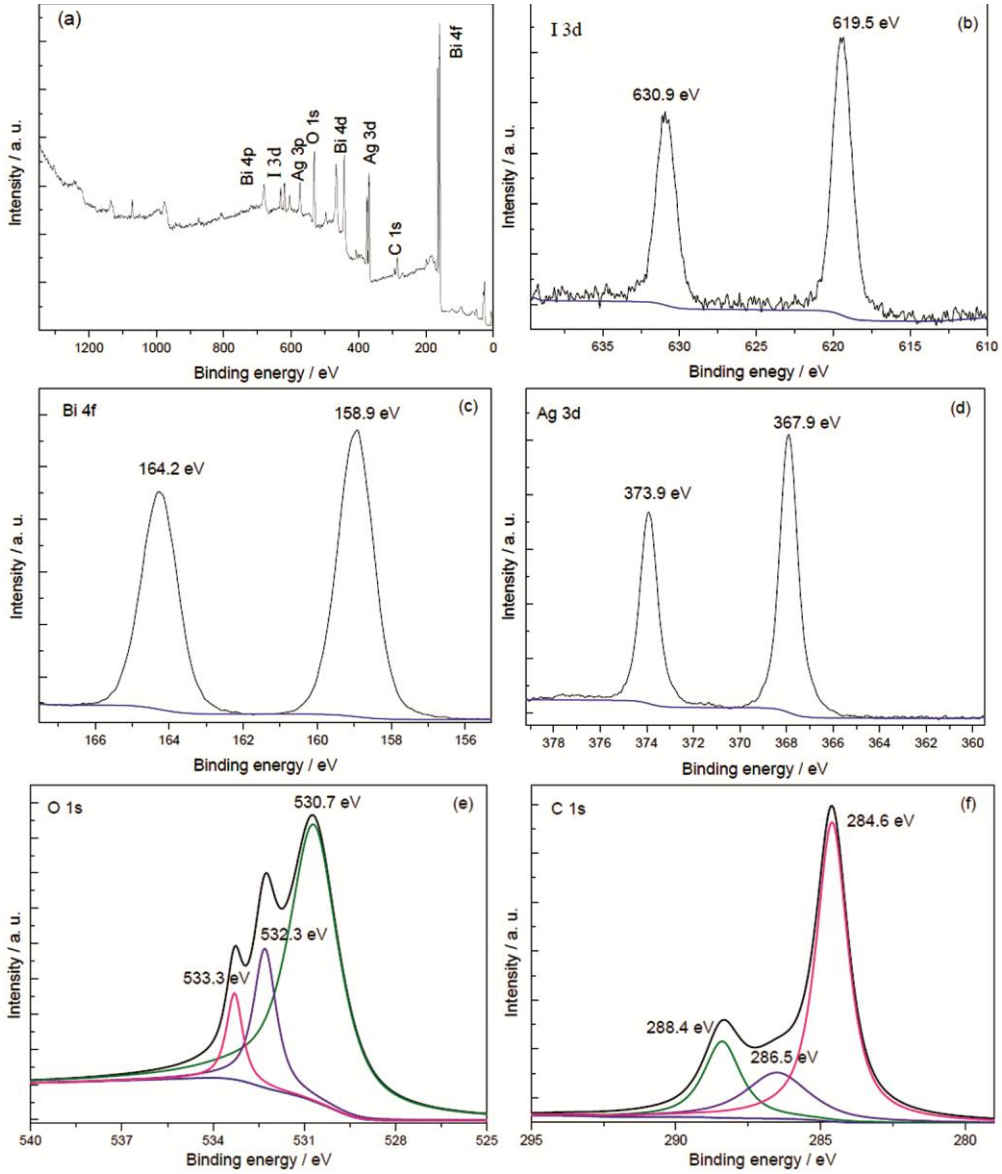

Fig. 3 — The survey profiles of (a) Ag_2CO_3/BiOI material and high-resolution XPS spectra of (b) I 3d, (c) Bi 4f, (d) Ag 3d, (e) O 1s and (f) C 1s.

eV was caused by absorbed oxygen species on catalyst surface and crystal lattice oxygen for Ag_2CO_3 component[23], whereas the peak appears at 530.7 eV was resulted from linkage of O–Bi[24]. The asymmetrical XPS profiles of C 1s could be divided into the following peaks. The shoulder peaks that appeared at 288.4 and 286.5 eV could be assigned to carbonate ion in Ag_2CO_3 particles, while the remaining peak located at 284.6 eV should belong to the adventitious carbon elements as well as the presence of C–C. Thus, the above results further revealed that Ag_2CO_3 was successfully composed with BiOI to form a bismuth oxyiodide/silver carbonate complex.

Physicochemical properties

Fig. 4(a) depicts the UV-vis diffuse reflection spectra (UV-vis DRS) of silver carbonate, pure BiOI and silver carbonate/BiOI composite. It can be seen from the graph that Ag_2CO_3 has excellent light absorption capability in the visible light region, and its absorption band edge was estimated to be 565 nm by extrapolation. In comparison, pure BiOI has significantly stronger and broad absorption capability than bare Ag_2CO_3 in the range of visible light, and its absorption band edge was estimated to be about 671 nm by extrapolation. After the two semiconductors are coupling, Ag_2CO_3/BiOI sample shows light absorption capability approximately situated in the wavelength of 480-620 nm, indicating that the Ag_2CO_3/BiOI sample was able to be sensitive in visible-light region. According to the intrinsic absorption peak of each sample absorption curve in the figure, the light absorption threshold value of the sample is obtained by taking the intersection point of the tangent line and the x axis, and then the band gap energy formula is employed to obtain band gap of samples. The band gap of semiconductor photocatalyst can be calculated according to the formula: $E_0 = 1240/\lambda_0$ (eV), where E_0 is the corresponding band gap and λ_0 is the optical absorption edge. Thus, the band gap of pristine Ag_2CO_3 and BiOI was determined to be 2.20 and 1.85 eV, respectively.

The steady-state PL spectra of samples were measured to acquire information on electron transition and transfer. As shown in Fig. 4(b), a fluorescence spectrum diagram was obtained by excitation of Ag_2CO_3, BiOI and Ag_2CO_3/BiOI complex under 420nm visible light. The broad emission peak of Ag_2CO_3 sample was located around at 550-680 nm, whereas emission peak of Ag_2CO_3 sample was mainly

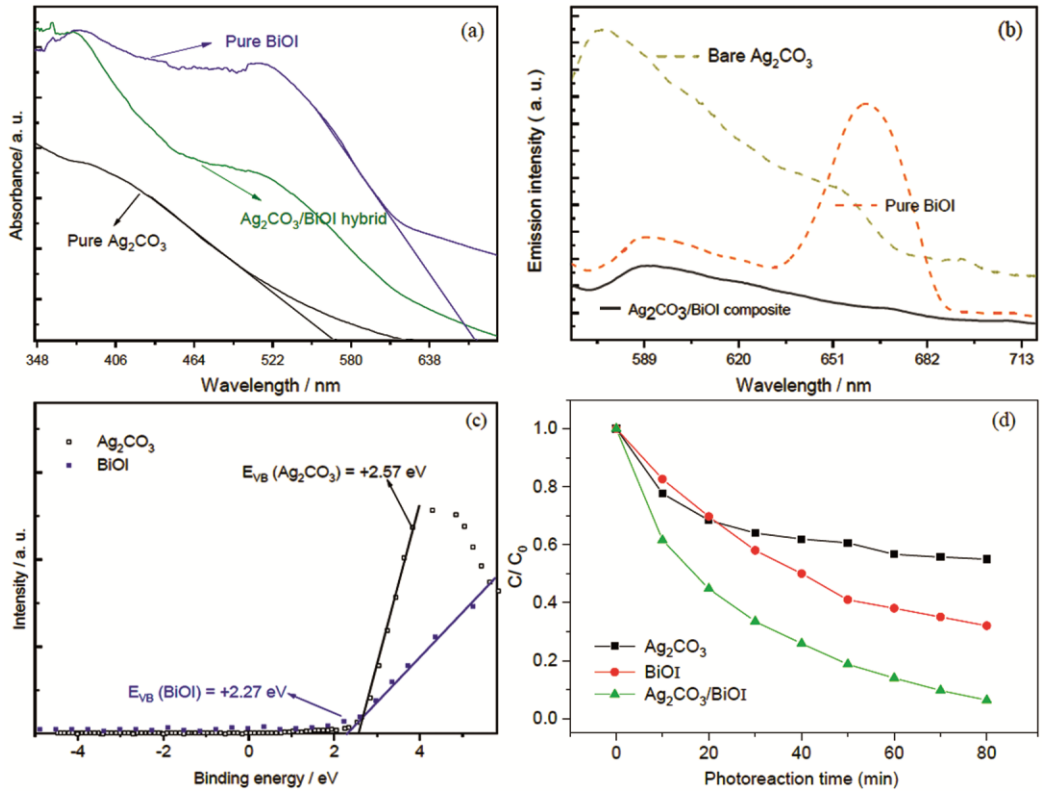

Fig. 4 — UV-vis diffuse reflection spectra (a), PL spectra (b), valence-band XPS spectra (c) and photocatalytic activities toward MO degradation (d) of pure Ag_2CO_3, BiOI and Ag_2CO_3/BiOI samples.

located around at 625-695 nm. Normally, lower the fluorescence emission intensity, lower the electron-hole recombination probability of the catalyst. From the graph, we can see that the fluorescence intensity of bare Ag_2CO_3 is the highest, while BiOI is slightly lower, and the fluorescence intensity of Ag_2CO_3/BiOI composite is the lowest, which is beneficial to the photocatalytic reaction. The peak intensities of Ag_2CO_3/BiOI composite dropped down compared with pure Ag_2CO_3 or BiOI. It is generally known that the lower intensity of catalysts means the lower combination rate of photo-induced electron-hole pairs. Hence, Ag_2CO_3/BiOI composite with the lowest PL intensity displayed the good performance in trapping photo-generated electrons, indicating that the combination of the two semiconductors may effectively reduce the coincidence rate of holes with photogenerated electrons.

Besides, valence band (VB) XPS spectra of the Ag_2CO_3 and BiOI were measured in order to investigate energy band positions. The VBs of Ag_2CO_3 and BiOI were measured based on valence-band XPS spectra (Fig. 4(c)). As depicted in graph, the VB energies (E_{VB}) of Ag_2CO_3 and BiOI samples can be drawn from the valance-band XPS spectra. The VB edge will be determined by linear extrapolation of the peaks to the baselines, thereby find the intercept with the linear fit and the edges of the maximum energy were found occur at approximately 2.57 and 2.30 eV, respectively. Thus, the value of E_{VB} was estimated to be +2.57 and +2.30 eV (at hydrogen scale) for Ag_2CO_3 and BiOI materials, respectively. The CB minima can be determined according to the optical band gaps. It can be concluded that the CB edge (E_{CB}) of pure BiOI and Ag_2CO_3 samples were +0.45 and +0.37eV (SHE as reference), respectively according to the equation of $E_0 = E_{VB} - E_{CB}$ along with the previous UV-vis DRS results.

Photocatalytic activity

The photocatalytic activity of BiOI, Ag_2CO_3 or Ag_2CO_3/BiOI material under visible light was investigated using degradation MO, phenol or PNA as the photocatalytic reaction model. Fig. 4(d) displays the results that under the action of different catalysts, which showing the photocatalytic degradation rate of BiOI, Ag_2CO_3 and Ag_2CO_3/BiOI samples to MO solution as a function of time. As can be seen, after 80 min of visible light irradiation, the degradation rates of Ag_2CO_3 and BiOI to methyl orange are about 45.0% and 68.0%, respectively. It is clear that pure Ag_2CO_3 basically has no remarkable photocatalytic degradation ability for dye and only < 50% of MO was bleached by single-phase Ag_2CO_3 during the same time. Pure BiOI has certain photocatalytic degradation capability for dye, because BiOI has stronger visible light absorption capability than that of Ag_2CO_3. When BiOI is coupled with Ag_2CO_3 to form Ag_2CO_3/BiOI composite, the degradation rate of MO is rapidly increased and the activity of the Ag_2CO_3/BiOI catalyst is the highest. Obviously, compared with Ag_2CO_3 and BiOI, the degradation rate of methyl orange by Ag_2CO_3/BiOI composite photocatalyst is significantly improved. Fig. 5(a) shows the degradation of aqueous MO solution under visible light illumination via BiOI. The change of UV-Vis absorption spectrum of MO solution can be detected during the continuous degradation by BiOI catalyst. With the increase of illumination time, the maximum absorption peak at 464 nm in the absorption spectrum rapidly decreases, suggesting that MO dye is gradually decomposed by photocatalysis. Fig. 5(b) gives the visible light photocatalytic activities of Ag_2CO_3/BiOI sample. As can be seen, the photocatalytic activity of Ag_2CO_3/BiOI composite was found to be better than the synthesized BiOI nanoparticle. After 80 min of degradation, the degradation rate of MO reaches 93.7%, which was 2~3 folds than BiOI or Ag_2CO_3 alone.

The photocatalytic activity was also estimated by other model pollutions such as phenol and PNA. As illustrated in Fig. 5(c),in the presence of bare Ag_2CO_3 or BiOI catalysts, 43% or 58% of phenol was degraded under visible-light irradiation in 60 min, respectively. However, obvious degradation of phenol was observed in the presence of composite material. The as-made Ag_2CO_3/BiOI material exhibited the highest photocatalytic efficiency, nearly 80% of phenol could be decomposed. Besides, Ag_2CO_3/BiOI material also can be applied for PNA removal, the PNA molecules were degraded greatly (~75%) by Ag_2CO_3/BiOI in 60 min (Fig.5d). For comparison, only 29% and 42% of PNA was degraded by pure Ag_2CO_3 or BiOI after 60 min of illumination, respectively, and the degradation rates were much lower than that of Ag_2CO_3/BiOI composite. To conclude, the composite has excellent activity to decompose either MO, phenol or PNA.

Photocatalytic mechanism

In the process of visible light degradation of model substrate, a series of active species participate in the photocatalytic reaction. The detection of reactive

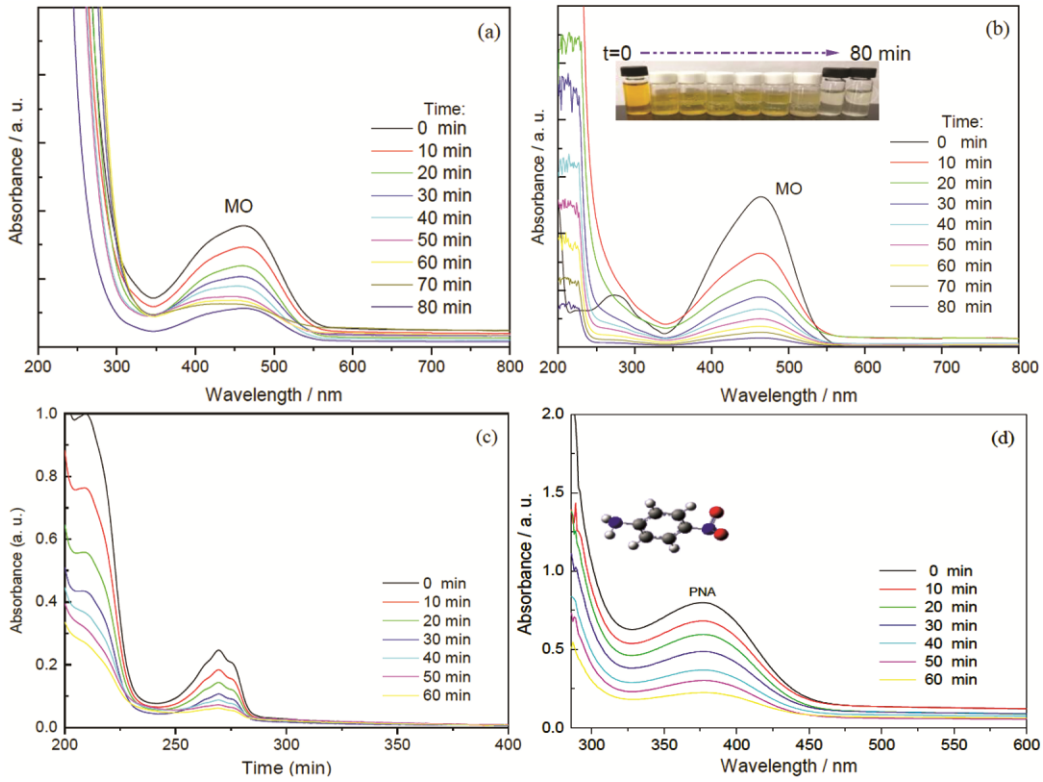

Fig. 5 — Temporal absorption spectra for MO degradation in the presence of BiOI (a) and Ag_2CO_3/BiOI composites (b), and absorption spectra of phenol (c) and PNA (d) aqueous solution in the presence of Ag_2CO_3/BiOI composite.

substances in photocatalytic process is the key to understand the mechanism of photocatalytic reaction. The active species capture test was carried out with the quencher at the concentration of 1.1 mmol/L. In detail, ascorbic acid, potassium iodide (KI), formic acid and potassium bichromate ($K_2Cr_2O_7$) were added into Ag_2CO_3/BiOI photocatalytic reaction system, which can be used as quenchers of hydroxyl radicals (*OH), holes (h+), superoxide radical anions (*O_2—) and free electrons (e—), respectively.

The influence of various capture agents on the photodegradation rate of methyl orange is demonstrated in the Fig. 6a. The results showed that the introduction of $K_2Cr_2O_7$ had no obvious inhibition on the degradation process of the reaction system.It confirms that photogenerated electrons (e—) are not the main active species in photocatalytic process since the photodegradation ability was not significantly affected. However, the photocatalytic activity was reduced in different degrees and the photocatalytic effect was inhibited after adding HCOOH and ascorbic acid (AA) in the experiment of photocatalytic degradation of MO. The photocatalytic degradation rate of MO is dropped to 60% and 40% after 80 min of illumination as HCOOH and AA were added, respectively. Meanwhile, when KI is added, the photocatalytic degradation rate of MO is also reduced. The photocatalytic degradation rate of MO is significantly reduced to 19% after 80 min of illumination, which proving that the number of active groups in it was reduced and captured. The results showed that the introduction of KI led to a significant reduction in the photocatalytic degradation effect of the system after 80 min of reaction compared with the sample without quencher, and the reduction was the most significant with the final degradation rate less than 20%. Summarize the above experimental facts, it can be speculated that e— was not the main active species of photocatalytic reaction, whereas h+ was the main active species and *OH or *O_2— active species play a secondary role in photocatalytic degradation system. Moreover, the photocatalytic activity almost disappeared after the capture agent KI was added, indicating that most of the photocatalytic system was captured by the capture agent and resulting in a decrease in the catalytic activity of the photocatalytic material. Therefore, h+ occupies a dominant position and acts a pivotal role in the current photocatalytic reaction system, and at the same time, there are some active groups such as *OH or *O_2—, which plays

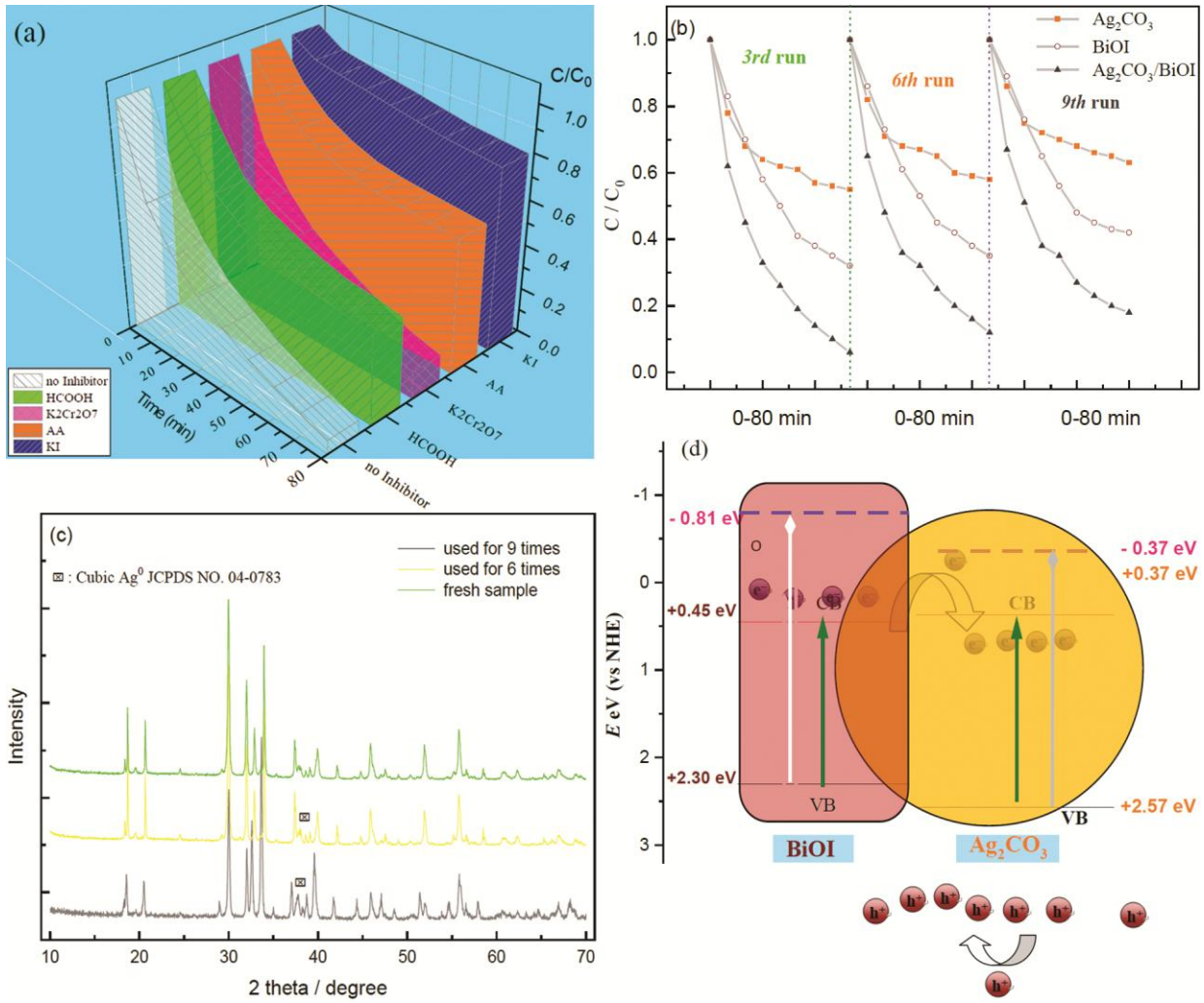

Fig. 6 — Effects of a series of inhibitors on the photocatalytic efficiency of Ag_2CO_3/BiOI composite material (a), recycling experiments for MO removal over Ag_2CO_3/BiOI composite (b), the XRD patterns (c) of Ag_2CO_3/BiOI composite before and after reuse for photo degrading MO and schematic diagram (d) of band alignment according to the determined E_{cb} and E_{vb} showing the energy band structure and charge transfer mechanism.

secondary role for photocatalytic degradation of pollutants.

As a photocatalyst, its stability is important in application. Fig. 6(b) compared the cyclic photocatalytic activity for MO photo degradation over these samples. After nine cycles, the photocatalytic degradation rate of the composite catalyst can be kept at a high level, indicating that the composite has good photocatalytic stability and reusability. By comparison, no more than 40% of MO was degraded by Ag_2CO_3 after 9 cycles. It could be seen that the cyclic photocatalytic performance of as-made Ag_2CO_3/BiOI composite is much higher than that of pure phase Ag_2CO_3 or BiOI, indicating that Ag_2CO_3/BiOI composite not only improve the photocatalytic activity of Ag_2CO_3, but also improve its stability. Moreover, the XRD of sample for recycling experiments have been measured to check the stability for the composite. Correspondingly, Fig. 6 (c) provides the XRD patterns of as-prepared Ag_2CO_3/BiOI composite before and after degradation of model pollutants. After six catalytic runs, the Ag^0 peak intensity at 38.1°C appeared and intensified with the recycle runs. However, the other peaks did not change compared with the fresh catalyst. The existence of metal Ag in the spent Ag_2CO_3/BiOI composite suggested that Ag_2CO_3 gradually changed into Ag^0 during the long-term photodegradation process. The change in chemical state of Ag species was possibly caused due to the combination of photogenerated electrons with Ag^+, which made the amounts of Ag gradually increase in photocatalytic

reactions. However, the coupling of BiOI significantly enhanced the photocatalytic activity of Ag_2CO_3, and the as-prepared Ag_2CO_3/BiOI composite exhibited the highest catalytic activity. Moreover, Ag_2CO_3/BiOI composite reduced the serious photocorrosion of Ag_2CO_3 and showed excellent catalytic recycling stability.

It is evident that the top of valence band (E_{VB}) of Ag_2CO_3 and BiOI samples were +2.57 and +2.30 eV (at hydrogen scale), whereas the original CB of BiOI and Ag_2CO_3 samples were +0.45 and +0.37 eV (SHE as reference), respectively. It can be seen that the valence band potential of Ag_2CO_3 is more positive than that of BiOI, where as the conduction band potentials are relatively close between each other although band potential of Ag_2CO_3 is more negative than that of BiOI. Therefore, they will form a heterojunction structure when they are combined together. According to the traditional heterojunction theory, photo induced holes generated after light excitation will migrate spontaneously from the valence band of Ag_2CO_3 to the valence band of BiOI since the potential of the valence band of Ag_2CO_3 is more positive than that of the valence band of BiOI. However, electrons transferred to the conduction band of BiOI or Ag_2CO_3 cannot react with O_2 to generate $*O_2—$ directly since CB is +0.37 eV for Ag_2CO_3 or +0.45 eV for BiOI, which is more positive than that of the standard redox potential of $*O_2—/O_2$ (-0.28 V vs. SHE). Nonetheless, it is likely that the VB edge of Ag_2CO_3 and BiOI could be excited a more negative CB potential edge of -0.38 and -0.65 eV under the excitation of employed visible-light source ($\lambda \geq 420$ nm), from which the behaviour is similar to the other photocatalytic system such as α-$SnWO_4$/SnO_2 heterostructure in previous literature studies[25]. The newly established CB potential edge could make electrons migrate from the CB of BiOIto that of Ag_2CO_3. Moreover, $*O_2—$ could formed due to the newly reformed CB of Ag_2CO_3 is more negative than standard redox potential of $*O_2—/O_2$ (-0.28 V vs. SHE). In addition, since the valence band potentials of Ag_2CO_3 and BiOI are relatively positive, and both valence bands are positive than *OH/OH— (+1.99 V, vs SHE) and $*OH/H_2O$ (+2.27 V, vs SHE) [44]. A small part of *OH in the active species capture experiment may come from the reaction of h+ with the surface hydroxyl of the catalyst itself or from the direct reaction of h+ with H_2O. On the other hand, the photo-excited holes in the VB of Ag_2CO_3 will drifted to the VB of BiOI according to the law of thermodynamics. The photoinduced holes that injected into the VB of BiOI still have sufficient oxidation ability since the VB band potential of BiOI is +2.30 eV, these holes in the VB of BiOI may be able to react with target molecules. Finally, repeated attacks of target molecules by oxidative h^+ in VB of BiOI and a small portion of *OH lead to successful degradation of MO, which is consistent with the fact that h^+ is a major active species in the reaction system in the light capture test. At the same time, the continuous consumption of h+ also promotes the separation efficiency of photogenerated electrons and holes and improves the reaction activity. In this case, photo induced electron-hole pairs are effectively separated, and the whole system has good transfer and separation capability of photo-generated electrons and holes. At the same time, the suitable energy band position of the system makes highly active holes and hydroxyl groups as active oxygen species enhance the oxidation ability of the composite system. The combination of BiOI and Ag_2CO_3 obviously improves the carrier mobility and can effectively promote the photocatalytic activity of Ag_2CO_3. It thus can be drawn that the photocatalytic activity enhancement of Ag_2CO_3/BiOI is attributed to the strong absorption in the visible region and the efficient charge separation owing to the matching band potentials between BiOI and Ag_2CO_3, as well as the low recombination rate of the electron-hole pairs due to the heterojunction formed between BiOI and Ag_2CO_3, which leading to the enhanced photocatalytic property.

Conclusion

In summary, visible-light responsive Ag_2CO_3/BiOI composite, Ag_2CO_3 nanoparticles and BiOI nanosheets have been prepared by solvo thermal approach. These catalysts have been tested for the photocatalytic degradation of various model pollutants under visible light. The superior photo degradation efficiency of Ag_2CO_3/BiOI is attributed to the formation of unique heterostructures with matched energy bands between Ag_2CO_3 nanoparticles and BiOI nanosheets. This can facilitate the transfer of electrons and increase the lifetime ofcarriers, resulting in superior photocatalytic degradation capability. It has been found that the main oxidizing species are holes and *OH or $*O_2—$play a secondary role. The recycle stability of the Ag_2CO_3/BiOI composite is tested and it is found that the

Ag_2CO_3/BiOI composite could preserve its crystal phase well during photocatalytic reaction. It is concluded that Ag_2CO_3/BiOI composite could nicely meet the requirements for ideal photocatalysts and exhibited enhanced activity in photocatalytic application. The present work may open up a new pathway for designing an effective photocatalyst with highly efficient catalytic performance for water remediation.

Acknowledgements

This work was supported by Science and Technology Innovation Fund for College Students (SRF) (Project no: 2021371).

References

1 Wan Z, Zhang G K, Wang J T & Zhang Y L, *RSC Adv*, 3 (2013) 19617.
2 Guo Y D, Zhang G K, Gan H H &Zhang Y L, *Dalton Trans*, 41 (2012) 12697.
3 Guo Y D, Zhang G K, Liu J & Zhang Y L, *RSC Adv*, 3 (2013) 2963.
4 Mu Y, Ai Z H & Zhang L Z, *Environ Sci Technol*, 51 (2017) 8101.
5 Wang L, Cao M H, Ai Z H &Zhang L Z, *Environ Sci Technol*, 48 (2014) 3354.
6 Qin Y X,Song F H, Ai Z H, Zhang P P & Zhang L Z, *Environ Sci Technol*, 49 (2015) 7948.
7 Chen N, Huang Y H, Hou X J, Ai Z H & Zhang L Z, *Environ Sci Technol*, 51 (2017) 11278.
8 Hu Y, Peng X, Ai Z H, Jia F L & Zhang L Z, *Environ Sci Technol*, 53 (2019) 8333.
9 Hou X J, Huang X P, Jia F L, Ai Z H, Zhao J C & Zhang L Z, *Environ Sci Technol*, 51 (2017) 5118.
10 Wang X G, Sun M H, Murugananthan M ,Zhang Y R & Zhang L Z , *Appl Catal B Environ*, 260 (2020) 118205.
11 Zhang G K, Gao Y Y, Zhang Y L & Guo Y D, *Environ Sci Technol*, 44 (2010) 6384.
12 Zhang Y L, Wang D J & Zhang G K, *Chem Eng J*, 173(2011) 1.
13 Zhang Y L, Gan H H & Zhang G K, *Chem Eng J*, 172 (2011) 936.
14 Zhang Y L, Deng L J, Zhang G K & Gan H H, *Colloid Surf A*, 384 (2011) 137.
15 Jiang J, Zhao K, Xiao X Y & Zhang L Z, *J Am Chem Soc*, 134 (2012) 4473.
16 Jiang J, Zhang L Z, Li H, He W W & Yin J J, *Nanoscale*, 5 (2013)10573.
17 Jiang J & Zhang L Z, *Chem Eur J*, 17 (2011) 3710.
18 Li H, Shi J G, Zhao K & Zhang L Z, *Nanoscale*, 6 (2014) 14168
19 Li J, Yu Y & Zhang L Z, *Nanoscale*, 6 (2014) 8473.
20 Li H & Zhang L Z, *Nanoscale*, 6 (2014) 7805.
21 Jiang J, Zhang X, Sun P B & Zhang L Z, *J Phys Chem C*, 115 (2011) 20555.
22 Zhang X & Zhang L Z, *J Phys Chem C*, 114 (2010) 18198.
23 Mehraj O, Mir N A, Pirzada B M, Sabir S & Muneer M, *J Mol Catal A Chem*, 395 (2014) 16.
24 Malathi A, Arunachalam P, Kirankumar V S, Madhavan J & Al-Mayouf A M, *Optic Mater*, 84 (2018) 227.
25 Yao S Y, Zhang M, Di J W, Wang Z S, Long Y M & Li W F, *Appl Surf Sci*, 357 (2015) 1528.